AD-A088 054 NAVAL RESEARCH LAB WASHINGTON DC F/G 20/7
DIOCOTRON INSTABILITY OF A RELATIVISTIC COAXIAL MULTI-RING HOLL--ETC(U)
AUG 80 H C CHEN, P J PALMADESSO
UNCLASSIFIED NRL-MR-4286 NL

1 OF 1
AD A088054

END
DATE FILMED
9-80
DTIC

AD A088054

(1) RR01107

SECURITY CLASSIFICATION OF THIS PAGE (When Data Entered)

(9) REPORT DOCUMENTATION PAGE

READ INSTRUCTIONS BEFORE COMPLETING FORM

1. REPORT NUMBER: N[redacted] Memorandum Report [redacted]	2. GOVT ACCESSION NO.: AD-A088054
3. RECIPIENT'S CATALOG NUMBER	
4. TITLE (and Subtitle): DIOCOTRON INSTABILITY OF A RELATIVISTIC COAXIAL MULTI-RING HOLLOW ELECTRON BEAM	5. TYPE OF REPORT & PERIOD COVERED: Interim report on a continuing NRL problem.
	6. PERFORMING ORG. REPORT NUMBER
7. AUTHOR(s): H.C. Chen* [redacted] P.J. Palmadesso	8. CONTRACT OR GRANT NUMBER(s): (12) 37
9. PERFORMING ORGANIZATION NAME AND ADDRESS: Naval Research Laboratory, Washington, D.C. 20375	10. PROGRAM ELEMENT, PROJECT, TASK AREA & WORK UNIT NUMBERS: 67-0906-0-0; (17) RR0110703; 51153N
11. CONTROLLING OFFICE NAME AND ADDRESS: Office of Naval Research, Arlington, Virginia 22217	12. REPORT DATE: (11) 18 Augu[redacted]80
	13. NUMBER OF PAGES: 29
14. MONITORING AGENCY NAME & ADDRESS (if different from Controlling Office): (14) NRL MR-4376	15. SECURITY CLASS. (of this report): UNCLASSIFIED
	15a. DECLASSIFICATION/DOWNGRADING SCHEDULE

16. DISTRIBUTION STATEMENT (of this Report)

Approved for public release; distribution unlimited.

17. DISTRIBUTION STATEMENT (of the abstract entered in Block 20, if different from Report)

DTIC ELECTE AUG 20 1980 S D B

18. SUPPLEMENTARY NOTES

*Science Applications, Inc.
McLean, Virginia 22102
This work was sponsored by the Office of Naval Research under project RR0110703.

19. KEY WORDS (Continue on reverse side if necessary and identify by block number)

Autoaccelerator
Diocotron instability
Relativistic electron beam
Hollow beam

20. ABSTRACT (Continue on reverse side if necessary and identify by block number)

The diocotron stability properties of a relativistic coaxial multi-ring hollow electron beam are investigated using a macroscopic cold fluid description based on moment-Maxwell equations. It is found that for a broad range of beam parameters and somewhat more general type beam profile the growth rate of instability has a sensitive dependence on fractional charge neutralization, relative position of the rings with conducting wall and gap-length of the rings. In the case of a sharp boundary density profile, the beam can be stabilized easily by a small fractional charge neutralization with appropriate gap-length. The growth rate can be either enhanced or reduced depending on the position and gap-length of the rings.

DD FORM 1 JAN 73 1473 EDITION OF 1 NOV 65 IS OBSOLETE
S/N 0102-LF-014-6601

 SECURITY CLASSIFICATION OF THIS PAGE (When Data Entered)

251950

TABLE OF CONTENTS

I.	INTRODUCTION	1
II.	BASIC THEORY	2
III.	STABILITY ANALYSIS	5
IV.	NUMERICAL RESULTS	8
V.	CONCLUSION	10
	ACKNOWLEDGEMENT	11
	REFERENCES	12

ACCESSION for
NTIS White Section
DDC Buff Section
UNANNOUNCED
JUSTIFICATION
BY
DISTRIBUTION/AVAILABILITY CODES
Dist. AVAIL. and/or SPECIAL
A

DIOCOTRON INSTABILITY OF A RELATIVISTIC COAXIAL MULTI-RING HOLLOW ELECTRON BEAM

I. Introduction

There has been considerable interest in recent years in the development of powerful relativistic electron beams.[1-3] Intense relativistic hollow electron beams have been used in the laboratory recently for high-power microwave generation[2], in electron ring accelerators and autoaccelerators[3]. . . etc.

The autoacceleration process is a collective acceleration mechanism for generating a high kinetic energy hollow electron beam. Such beams are often designed to have approximately uniform electron density within an annular space near the wall of a cylindrical drift tube, with no electrons outside the annulus. Previous theoretical studies of the diocotron instability in hollow beams have assumed a beam profile of this type.

We have considered a somewhat more general type beam profile, namely a hollow coaxial multi-ring electron beam. Using a macroscopic cold fluid model, the diocotron instability which characterizes a hollow multi-ring electron beam has been investigated for a broad range of beam parameters and different geometries. Significantly different results exist between the multi-ring and single-ring hollow beams. Description of these differences is the purpose of this paper.

The basic theory and assumptions are described and equilibrium properties of the beam are examined in Section II. In Section III we confine our study to systems exhibiting linear behavior from which an eigenvalue equation for the perturbed potential is derived; In the case of a square radial density profile a closed algebraic dispersion relation for the complex eigenfrequency is extracted. The dispersion

Manuscript submitted June 4, 1980

relation is solved numerically in Section IV and stability properties are investigated in detail. Conclusions are drawn in Section V.

II. Basic theory

We start by considering a two-ring electron hollow beam with a smooth perfectly conducting wall as shown in Fig. 1. Analysis of dynamic properties is based on a macroscopic cold fluid model which is idealized in that the flow is laminar and there is no variation in the axial direction.[4] We assume a system infinite in the axial direction, and a strong uniform background magnetic field which prevents the beam from spreading. We consider a cylindrically symmetrical electron beam containing n electrons per unit volume moving along a strong axial magnetic field in a conducting drift tube at low pressure so that the beam is neither current nor charge neutralized. Two components are assumed, ions with charge q have no component of velocity along the beam and electrons move with velocity $\beta c\ \hat{e}_z$ which is assumed large compared with the transverse velocity. We allow partial neutralization by a fraction f of charges of opposite sign trapped in the beam. The neutralization fraction f denoting the ratio of neutralizing charge to beam charge is assumed uniform across the beam. By virtue of these assumptions the electrons are described in cylindrical geometry (r, θ, z) as a macroscopic cold fluid immersed in a uniform axial magnetic field $B_o\ \hat{e}_z$ with both radial space-charge and azimuthal self-magnetic fields included. The continuity equation and the equation of motion for the electron fluid can be expressed in the relativistic form as

$$\partial n/\partial t + \nabla \cdot (n\underline{V}) = 0 \tag{1}$$

$$(\partial/\partial t + \underline{V} \cdot \nabla)\ \gamma m \underline{V} = q(\underline{E} + \underline{V} \times \underline{B}) \tag{2}$$

where $n(\underline{x},t)$ and $\underline{V}(\underline{x},t)$ are the density and mean velocity and $\underline{E}(\underline{x},t)$ and $\underline{B}(\underline{x},t)$ are the electric and magnetic fields respectively. q and m are the charge and rest mass of the electron and $\gamma \equiv (1-\beta^2)^{-\frac{1}{2}}$ and $\beta \equiv v_b/c$ are the standard relativistic quantities and c is the velocity of light in vacuum. The system can be closed by adding Poisson's equation and Ampere's law as shown below respectively.

$$\nabla \cdot \underline{E} = \varepsilon_o^{-1} (1-f)\ q\ n \tag{3}$$

$$\nabla \times \underline{B} = \mu_o\ q\ \beta\ c\ n\ \hat{e}_z + \mu_o \varepsilon_o\ \partial \underline{E}/\partial t \tag{4}$$

where μ_o and ε_o are permeability and permittivity of free space.

The equilibrium state $(\partial/\partial t = 0)$ is azimuthally symmetric $(\partial/\partial\theta = 0$ and $\partial/\partial z = 0)$ and is characterized by electron density $n(r)$ and azimuthal electron fluid velocity $V_\theta\ \hat{e}_\theta$. The deviation from charge neutrality produces a radial electric field that influences the azimuthal motion of the electron fluid. In the case of a sharp-boundary equilibrium in which the electrons have a double rectangular density profile as shown in Fig. 2, where $r = R_c$ is the radial location of a grounded conducting wall, the self-generated radial electric and azimuthal fields can be obtained by integrating equations (3) and (4). Thus,

$$E_r(r) = (1-f)\beta^{-1}B_\theta(r)$$

$$= \frac{1}{2\varepsilon_o}\ q\ n(1-f)\begin{cases} (r^2 - R_1{}^2)/r & R_1 < r < R_2 \\ (R_2{}^2 - R_1{}^2)/r & R_2 < r < R_3 \\ (R_2{}^2 - R_1{}^2 + r^2 - R_3{}^2)/r & R_3 < r < R_4 \\ (R_2{}^2 - R_1{}^2 + R_4{}^2 - R_3{}^2)/r & R_4 < r < R_c \end{cases} \tag{5}$$

The radial electric field arising from the space charge has been reduced by a factor of (1-f) because the effect of partial neutralization by ions. It follows from Eq. (2) that equilibrium force balance in the radial direction can be expressed as

$$-\gamma m\frac{V_\theta{}^2}{r} = q(E_r + V_\theta B_o - \beta c\ B_\theta) \tag{6}$$

Eq. (6) is simply a statement of radial force balance of centrifugal, magnetic and electric forces on an electron fluid element. The self-magnetic field produces a force towards the axis which is weaker than the outward radial electrostatic force. The balance among electric, centrifugal and magnetic forces gives the angular velocity $\omega_b(r)$ of an electron fluid element in slow rotational equilibrium

$$\omega_b(r) \equiv \frac{V_\theta}{r} = \frac{\omega_{pb}{}^2}{\omega_{cb}}\ \frac{1-\gamma^2 f}{2\gamma^2}\begin{cases} (r^2 - R_1{}^2)/r^2 & R_1 < r < R_2 \\ (R_2{}^2 - R_1{}^2 + r^2 - R_3{}^2)/r^2 & R_3 < r < R_4 \end{cases} \tag{7}$$

where ω_{cb} and ω_{pb} are the electron cyclotron and plasma frequencies respectively. ω_b can be permitted to depend on r, giving sheared cold fluid rotation rather than rigid rotation. Laminar flow and the assumption of azimuthal symmetry together imply that individual charges moves in helices of constant radius.

III. Stability analysis

We assume all the perturbed quantities satisfy the conditions $\partial[\ ]/\partial z = 0$, $\partial[\ ]/\partial t = i\omega[\ ]$, and $\partial[\ ]/\partial\theta = -i\ell[\ ]$ with $\mathrm{Im}(\omega) < 0$, where ℓ is the azimuthal harmonic number. After Fourier decomposing the fluid-Maxwell equations (1) to (4), it is straightforward to show that in the strong magnetic field regime $\omega_{cb} \gg \omega_{pb}$ the eigenvalue equation for the perturbed field has the form

$$\left(\frac{1}{r}\frac{\partial}{\partial r} r \frac{\partial}{\partial r} - \frac{\ell^2}{r^2}\right)\delta\varphi(r) = \frac{-2\ell\,\delta\varphi(r)\left[\delta(r-R_1) - \delta(r-R_2) + \delta(r-R_3) - \delta(r-R_4)\right]}{r\left[\dfrac{\omega}{\omega_D} - \dfrac{\ell\omega_b(r)}{\omega_D}\right]} \tag{8}$$

where the perturbed potential $\delta\varphi(r) = \delta\phi(r) - \beta\,\delta A_z(r)$, ϕ and A are the scalar and vector potentials of the electromagnetic field, the diocotron frequency is defined by $\omega_D \equiv \omega_{pb}{}^2/2\gamma^2\omega_{cb}$, and $\omega_b(r)$ was given in (7). The right-hand side of the eigenvalue Eq. (8) is equal to zero except at the surface of the beam. Moreover, the eigenfunction $\delta\varphi(r)$ satisfies the vacuum Poisson equation except at $r = R_1$, R_2, R_3 and R_4, therefore the piece-wise solution for the homogeneous equation can be expressed as

$$\delta\varphi(r) = \begin{cases} a\, r^{\ell} + b\, r^{-\ell} & 0 < r < R_1 \\ c\, r^{\ell} + d\, r^{-\ell} & R_1 < r < R_2 \\ e\, r^{\ell} + f\, r^{-\ell} & R_2 < r < R_3 \\ g\, r^{\ell} + h\, r^{-\ell} & R_3 < r < R_4 \\ i\, r^{\ell} + j\, r^{-\ell} & R_4 < r < R_c \end{cases} \tag{9}$$

The ten coefficients are functions of R_1, R_2, R_3 . . . R_c to be determined by the boundary conditions, the requirement implied by delta functions. The eigenfunction is continuous at each boundary and vanishes both at $r = 0$ and $r = R_c$. The effect of the delta function can be considered by multiplying both sides by r and integrating over the infinitesimal interval from $r(1-\varepsilon)$ to $r(1 + \varepsilon)$ with $\varepsilon \to 0$ in the vicinity of $r = R_1$, R_2, R_3 and R_4 respectively. Therefore we have the following dispersion relation given by 10 equations with 10 unknowns

$$
\begin{aligned}
& b = 0 \\
& a\, R_1^{\ell} + b\, R_1^{-\ell} = c\, R_1^{\ell} + d\, R_1^{\ell} \\
& c\, R_1^{\ell} - d\, R_1^{-\ell} - a\, R_1^{\ell} + b\, R_1^{-\ell} = \frac{-2(a\, R_1^{\ell} + b\, R_1^{-\ell})}{\frac{\omega}{\omega_D}} \\
& c\, R_2^{\ell} + d\, R_2^{-\ell} = e\, R_2^{\ell} + f\, R_2^{-\ell} \\
& e\, R_2^{\ell} - f\, R_2^{-\ell} - c\, R_2^{\ell} + d\, R_2^{-\ell} = \frac{2(c\, R_2^{\ell} + d\, R_2^{-\ell})}{\frac{\omega}{\omega_D} - Y_1} \\
& e\, R_3^{\ell} + f\, R_3^{-\ell} = g\, R_3^{\ell} + h\, R_3^{-\ell} \\
& g\, R_3^{\ell} - h\, R_3^{-\ell} - e\, R_3^{\ell} + f\, R_3^{-\ell} = \frac{-2(e\, R_3^{\ell} + f\, R_3^{-\ell})}{\frac{\omega}{\omega_D} - Y_2} \\
& g\, R_4^{\ell} + h\, R_4^{-\ell} = i\, R_4^{\ell} + j\, R_4^{-\ell} \\
& i\, R_4^{\ell} - j\, R_4^{-\ell} - g\, R_4^{\ell} + h\, R_4^{-\ell} = \frac{2(g\, R_4^{\ell} + h\, R_4^{-\ell})}{\frac{\omega}{\omega_D} - Y_3} \\
& i\, R_c^{\ell} + j\, R_c^{-\ell} = 0
\end{aligned}
\tag{10}
$$

where $Y_1 = (1-\gamma^2 f)\ (R_2^{\ 2} - R_1^{\ 2})/R_2^{\ 2}$

$Y_2 = (1-\gamma^2 f)\ (R_2^{\ 2} - R_1^{\ 2})/R_3^{\ 2}$

$Y_3 = (1-\gamma^2 f)\ (R_4^{\ 2} - R_3^{\ 2} + R_2^{\ 2} - R_1^{\ 2})/R_4^{\ 2}$

The determinant of the 10 linear equations gives the dispersion relation of the form

$$\left(\frac{\omega}{\omega_D}\right)^4 + c_1\left(\frac{\omega}{\omega_D}\right)^3 + c_2\left(\frac{\omega}{\omega_D}\right)^2 + c_3\left(\frac{\omega}{\omega_D}\right) + c_4 = 0 \qquad (11)$$

where

$$c_1 = R_{1c} - R_{2c} + R_{3c} - R_{4c} - Y_1 - Y_2 - Y_3$$

$$\begin{aligned} c_2 = {} & R_{12} - R_{13} + R_{14} + R_{23} - R_{24} + R_{34} + Y_1 - Y_2 + Y_3 - 2 + Y_1Y_2 \\ & + Y_2Y_3 + Y_1Y_3 - R_{1c}(1 + Y_1 + Y_2 + Y_3) + R_{2c}(1 + Y_2 + Y_3) \\ & - R_{3c}(1 + Y_1 + Y_3) + R_{4c}(1 + Y_1 + Y_2) \end{aligned}$$

$$\begin{aligned} c_3 = {} & Y_1 + Y_2 + Y_3 - 2Y_1Y_3 - Y_1Y_2Y_3 - R_{12}(Y_2 + Y_3) + R_{13}(Y_1 + Y_3) \\ & - R_{14}(Y_1 + Y_2) - R_{23}Y_3 + R_{24}Y_2 - R_{34}Y_1 - R_{1c}(1 - 2Y_2 - Y_1Y_2 \\ & - Y_1Y_3 - Y_2Y_3 - R_{43}) + R_{2c}(1 - 2Y_2 - Y_2Y_3 - R_{43}) \\ & - R_{3c}(1 - 2Y_1 - Y_1Y_3 - R_{12}) + R_{4c}(1 - 2Y_1 - Y_1Y_2 - R_{12}) \end{aligned}$$

$$\begin{aligned} c_4 = {} & (Y_1 - 1)(Y_2 + 1)(Y_3 - 1) + R_{1c}[(1 + Y_1)(1 - Y_2)(1 + Y_3) \\ & - (1 + Y_1)R_{43}] - R_{2c}[(1 - Y_2)(1 + Y_3) - R_{43}] \\ & - R_{3c}(1 + Y_3)(Y_1 - 1 + R_{12}) + R_{4c}(1 + Y_2)(Y_1 - 1 + R_{12}) \\ & - R_{12}[(Y_2 + 1)(Y_3 - 1) - R_{34}] + R_{13}(1 + Y_1)(1 - Y_3) \\ & - R_{14}(1 - Y_2)(1 + Y_1) - R_{23}(1 - Y_3) + R_{24}(1 - Y_2) + R_{34}(Y_1 - 1) \end{aligned}$$

where R_{ab} denoting the ratio of $R_a^{\ 2\ell}$ to $R_b^{\ 2\ell}$. If we let $R_2 = R_3$ then

Eq. (11) gives the results of mono-ring hollow beam case as shown in Uhm and Siambis[6]. By the methods analogous to those represented, it is straightforward to extend the case to multi-ring beams.

IV. Numerical results

It is concluded in Section III that the dispersion relation has quadratic form for the single-ring case and quartic for two rings, and so on; i.e., the order of the polynomial equation is twice the number of rings. The dispersion relation (11) is solved numerically for the complex eigenfrequency $\omega \equiv \omega_r + i\omega_i$ with real oscillation frequency ω_r and growth rate ω_i for the unstable mode. One important feature of Eq. (11) is that the complex eigenfrequency is linearly proportional to the diocotron frequency. Consequently the applied magnetic field strongly reduces the growth rate for fixed beam density. As a result, it is more instructive to keep the beam and plasma parameters fixed and study the growth rates for different geometries. Fig. 3 shows the growth rate for a two-ring beam versus gap-length d of the rings for different mode numbers ℓ and specified values of f. The gap-length d is defined as the distance between R_2 and R_3 while we fix the position R_1 and R_4 and keep the beamwidth of each ring identical. The total current of the beam has been held constant for various geometries so that the growth rates are evaluated at the same beam energy. As we can expect from Eq. (10) the growth rate has a strong dependence on $\gamma^2 f$. For simplicity we specify $\gamma = 2$ and show values of f on each curve. Note that the zero gap case is equivalent to a single-ring which is always stable for mode $\ell = 1$ as observed by Uhm and Siambis[6]. Therefore,

beams with various gap-length will destabilize the $\ell = 1$ mode at least for $.04 > F > .005$ as can be seen easily from Fig. 3. Note that there is no instability for the $\ell = 1$ mode when $f = 0$. The growth rate is higher for larger mode numbers ; For $\ell \geq 2$ the growth rate remains almost constant for $f = 0$ while the growth rate decreases rapidly as the fractional charge neutralization f is increased, i.e., the unstable modes can be stabilized easily by a small fractional charge neutralization with appropriate gap-length. By the way, the real frequency for the unstable modes shown in Fig. 3 is larger for higher ℓ but does not exceed $.6\ \omega_D$. It has been demonstrated that the growth rate of the instability exhibits a sensitive dependence on f. Neutralization is commonly produced from the residual gas in the apparatus. It is difficult to give a universal theory[8] for f which depends very much on such factors as the energy of the beam and the composition and pressure of the residual gases, ionization cross section, the energy of the secondary electrons and whether the ion can escape from the end of the beam.

Another interesting feature is that for higher modes the double region in gap-length for instability disappears from Fig. 3 to Fig. 4. Generally, the unstable mode for a single ring can be stabilized by increasing the gap-length of a two-ring beam in this kind of geometry. Next, we want to demonstrate the effect of the total beamwidth ($R_4 - R_1$) on the diocotron instability which is illustrated in Fig. 5 and Fig. 6. The $\ell = 1$ mode is unstable as before when the single-ring beam becomes a two-ring beam as shown in Fig. 5. However, the fundamental mode can no longer occur if the total beamwidth has expanded to

the one as shown in Fig. 6. Clearly, the $\ell = 1$ mode can be destabilized by moving two rings together. For $\ell \gtrsim 2$, the growth rate increases with respect to gap-length when $f = 0$; Nevertheless, the growth rate for small f increases with respect to gap-length first and then decreases sharply.

Finally, it is straightforward to extend the analysis to a three-ring geometry as shown in Fig. 7. For easy comparison between the two-ring and three-ring cases, we plot the growth rate versus gap-length $d \equiv (R_5 - R_2)$ while fixing the positions R_1 and R_6 and keeping the beam-width of each ring identical, the total current is also fixed. The effect of inserting the center ring can be seen easily while comparing Fig. 8 to Fig. 3. The unstable modes in two-ring geometry have been retained in the three-ring case, but also the growth rate has been enhanced by inserting the third ring in the middle, which may be caused by the strong coupling among the self-fields of the beams. For higher mode numbers, unstable modes can be found in three separate regions in gap-length domain. If we move the outer edge of the beam away from the wall, Fig. 9 gives the geometry which can be compared to Fig. 6. It comes as no surprise that the $\ell = 1$ mode becomes unstable again. For higher modes, the triple region for instability is not obviously seen; The conducting wall plays an important role in the diocotron instability.

V. Conclusion

We have formulated a fluid-Maxwell theory of the diocotron instability in an infinitely long relativistic electron beam propagating parallel to a uniform applied axial magnetic field. In beams with

self-fields it frequently permits simple models which illustrate many of the essential features of more realistic types of beam. The growth rate has been calculated with special emphasis put on displaying results as a function of conducting wall geometry, i.e., conducting wall location relative to the beams position. The results show the strong influence of neutralization fraction f, relative position of the rings with conducting wall and gap-length of the rings on the diocotron instability. It seems the instability has been enhanced by the multi-ring geometry in a rather complicated manner. In short, the $\ell = 1$ mode which is always stable in the single-ring case can become unstable in the multi-ring geometries. However, in the two-ring geometry, the $\ell = 1$ mode diocotron instability can be avoided by either moving two hollow beams away from the wall or spreading the two rings farther apart. For the $\ell \geq 2$ modes, the growth rate can be either enhanced (e.g. Fig. 5 and Fig. 6) or reduced (e.g. Fig. 3 and Fig. 4) depending on the position and gap-length of the rings. In the three-ring case, all the unstable modes occurring in the two-ring geometries have been retained and the growth rates have been enhanced at the same gap-length.

ACKNOWLEDGEMENT

This work was supported by the Office of Naval Research.

References

[1] Chapin, D. L. and J. J. Duderstadt, Phys. Fluids 18, 325 (1975).

Greenspan, M. A., C. Ekdahl, J. D. Sethian, and C. B. Wharton, Phys. Fluids 23, 205 (1980).

[2] Granatstein, V. L., P. Sprangle, M. Herndon, R. K. Parker and S. P. Schlesinger, J. Appl. Phys., 46, 3800 (1975).

[3] Siambis, J. G. and M. Friedman, Part. Accel., 8, 217 (1978).

Lockner, T. R. and M. Friedman, IEEE Trans. NS-26, 4238 (1979).

Siambis, J. G., Phys. Fluids 19, 1784 (1976).

[4] Lawson, J. D., "The Physics of Charges-Particle Beams", Clarendon Press, Oxford, 1977.

[5] Davidson, R. C., "Theory of Non-Neutral Plasmas", Benjamin, Reading, Mass., 1974.

[6] Uhm, H. S. and J. G. Siambis, Phys. Fluids 22, 2377 (1979).

[7] Conte, S. D. and C. Boor, "Elementary Numerical Analysis", McGraw-Hill, 1965.

[8] Engel, A. V. and M. Steenbeck, "Electrische Gasentladungen", Springer, Berlin, 1932.

Druyvesteyn, M. J. and F. M. Penning, Rev. Mod. Phys. 12, 87 (1940).

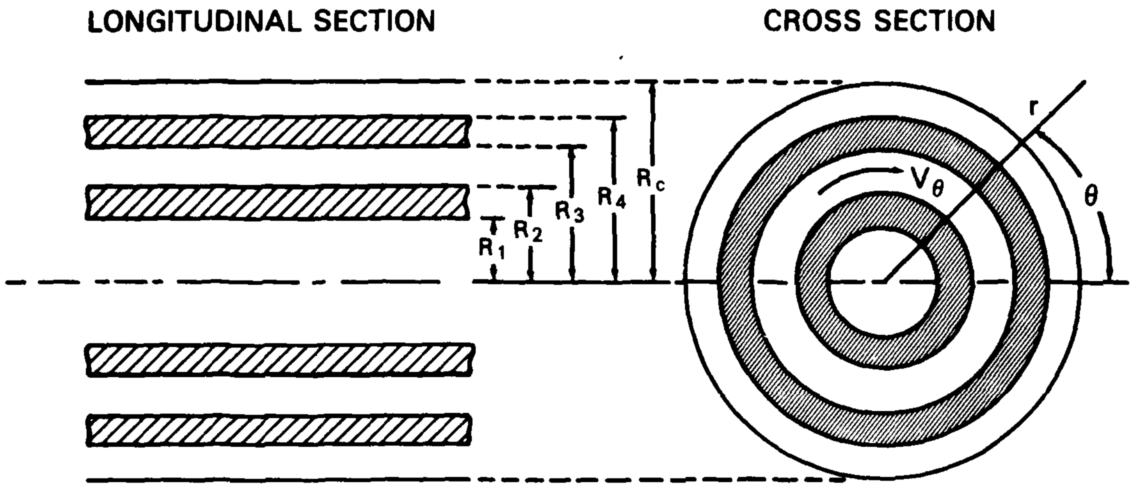

Fig. 1 - Longitudinal and cross section of equilibrium configuration and coordinate system

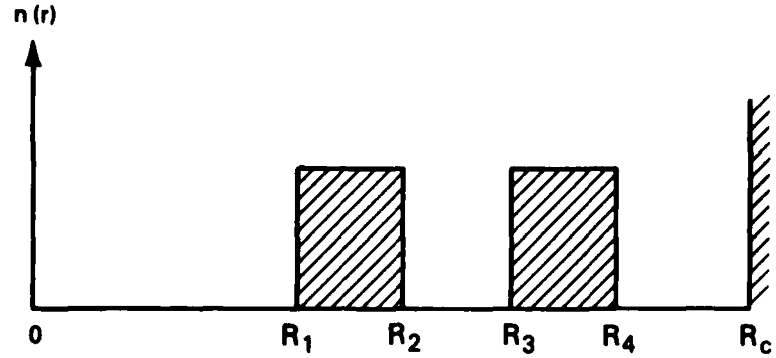

Fig. 2 - Beam electron density profile for two-ring geometry

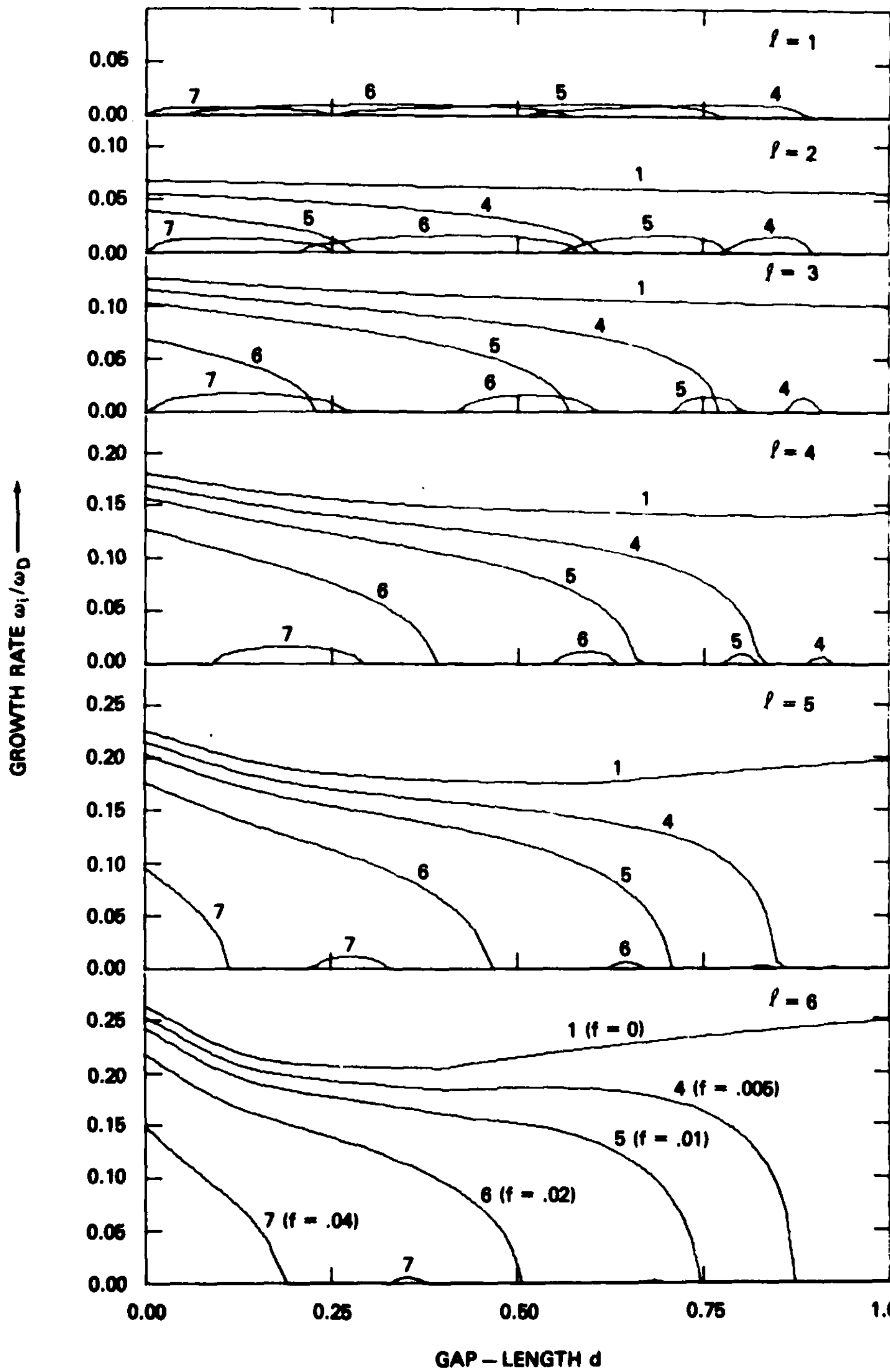

Fig. 3 - Growth rate ω_i/ω_D versus gap-length $d = (R_3 - R_2)/(R_4 - R_1)$ for $R_1 = .84\ R_c$, $R_4 = .92\ R_c$ ($\omega_r < .6\ \omega_D$)

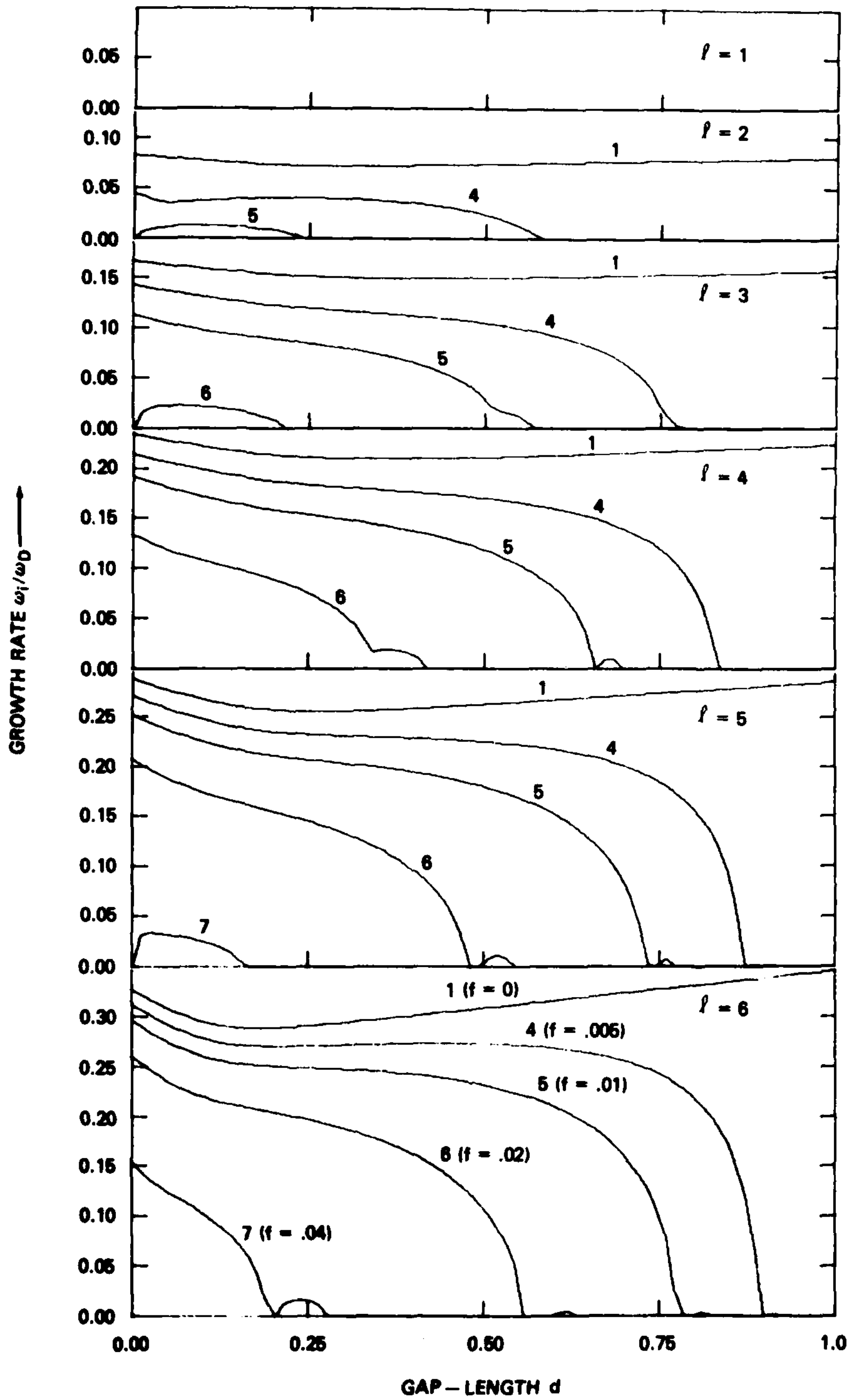

Fig. 4 - Growth rate ω_i/ω_D versus gap-length d =$(R_3 - R_2)/(R_4 - R_1)$ for $R_1 = .64\ R_c$, $R_4 = .72\ R_c$

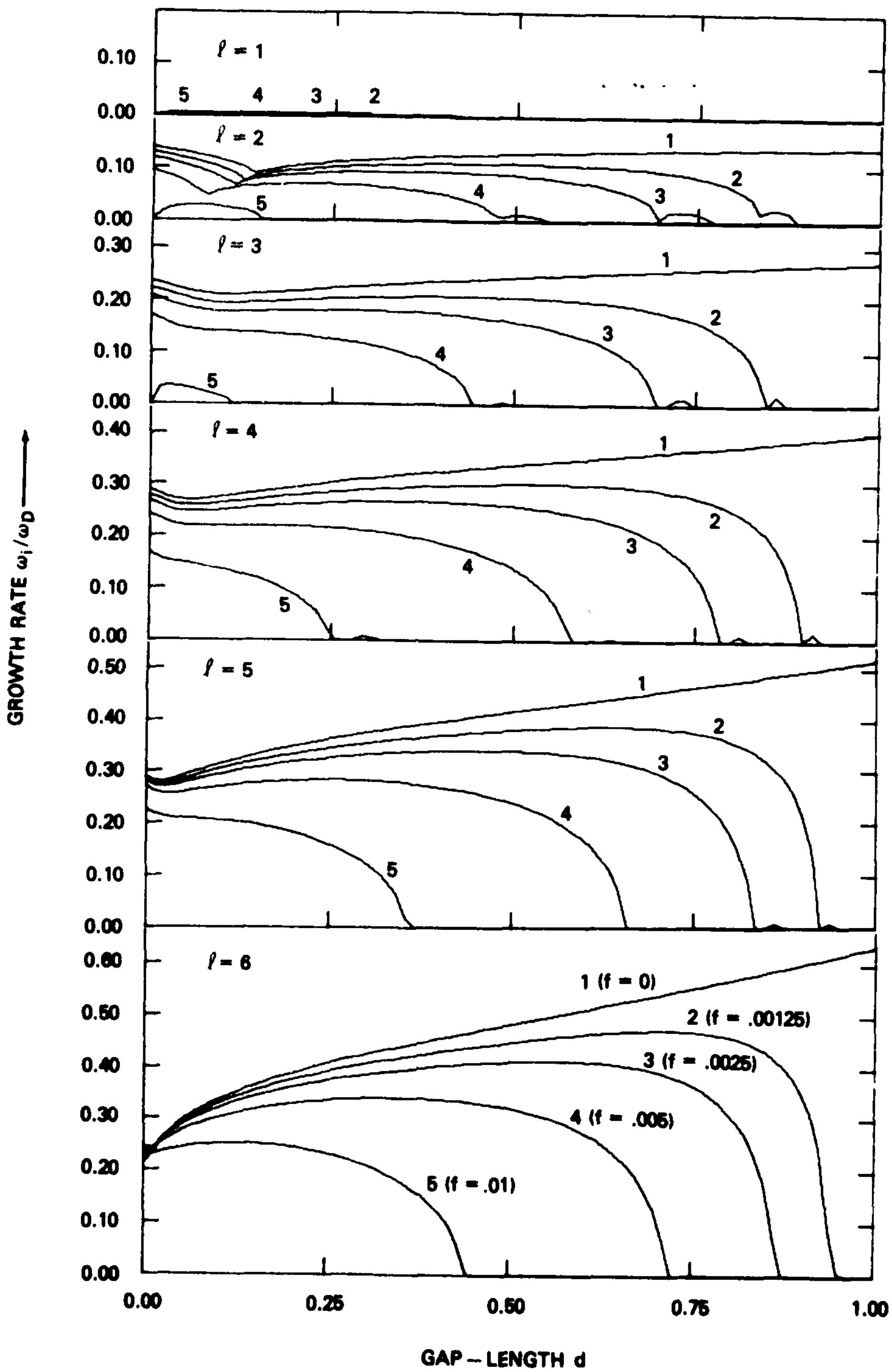

Fig. 5 - Growth rate ω_i/ω_D versus gap-length $d = (R_3 - R_2)/(R_4 - R_1)$ for $R_1 = .64\ R_c$, $R_4 = .8\ R_c$

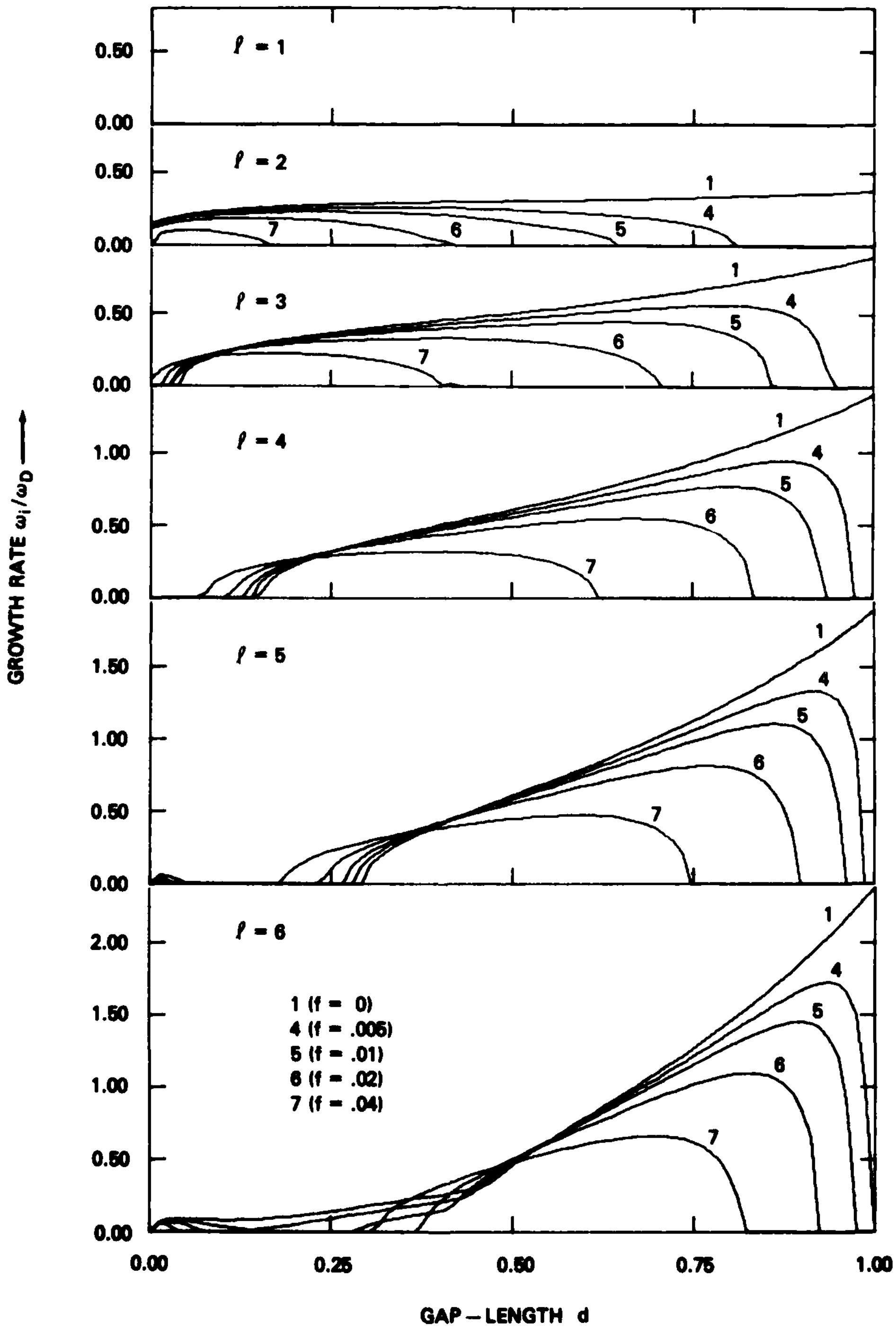

Fig. 6 - Growth rate ω_i/ω_D versus gap-length $d = (R_3 - R_2)/(R_4 - R_1)$ for $R_1 = .4\ R_c$, $R_4 = .8\ R_c$

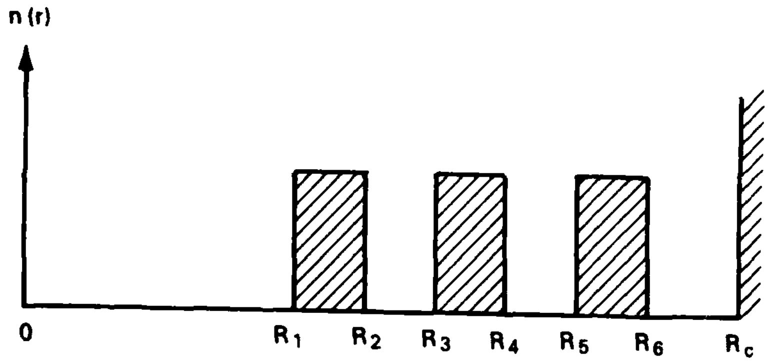

Fig. 7 - Beam electron density profile for three-ring geometry

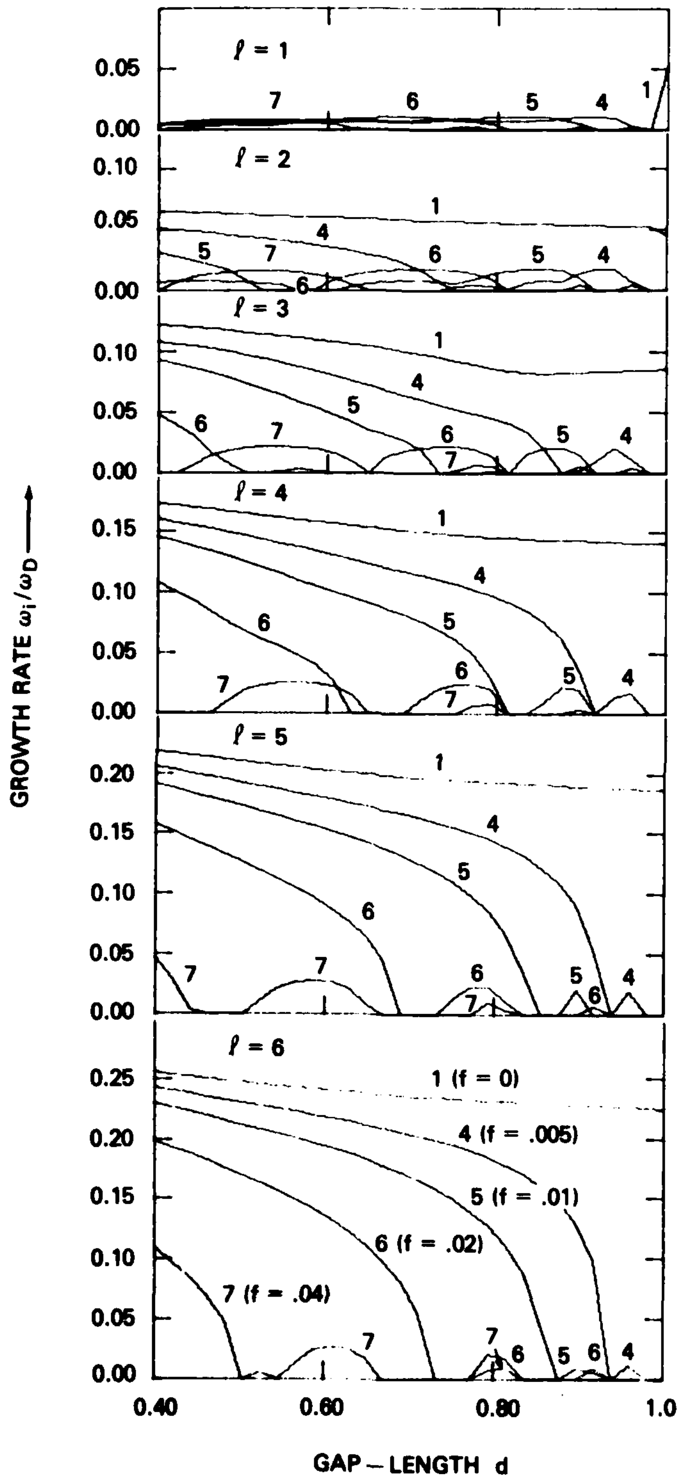

Fig. 8 - Growth rate ω_i/ω_D versus gap-length $d = (R_5 - R_2)/(R_6 - R_1)$ for $R_1 = .84\ R_c$, $R_6 = .92\ R_c$

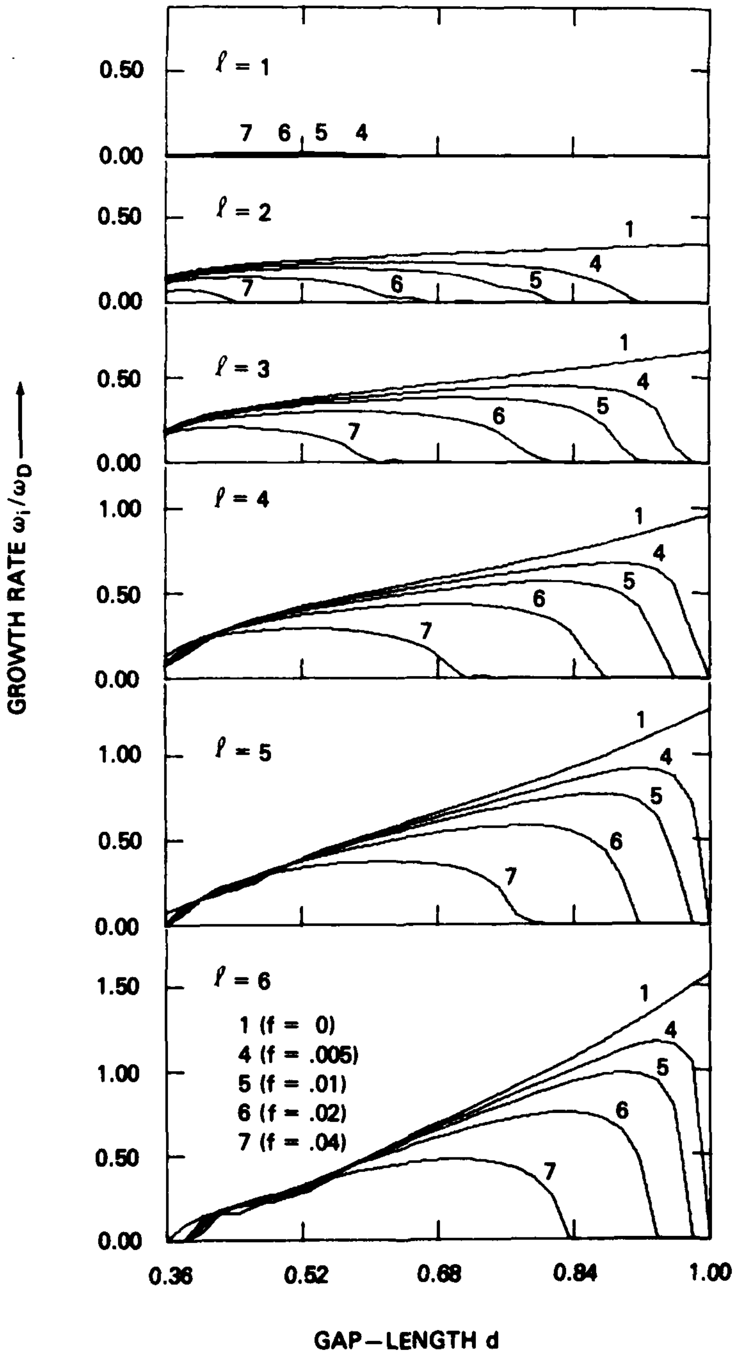

Fig. 9 - Growth rate ω_i/ω_D versus gap-length $d = (R_5 - R_2)/(R_6 - R_1)$ for $R_1 = .4\ R_c$, $R_6 = .8\ R_c$

DISTRIBUTION LIST

1. Commander
   Naval Sea Systems Command
   Department of the Navy
   Washington, D. C. 20363
   Attn: NAVSEA 03H (Dr. C. F. Sharn)

2. Central Intelligence Agency
   P. O. Box 1925
   Washington, D. C. 20013
   Attn: Dr. C. Miller/OSI

3. Air Force Weapons Laboratory
   Kirtland Air Force Base
   Albuquerque, New Mexico 87117
   Attn: Lt. Col. J. H. Havey

4. U. S. Army Ballistic Research Laboratory
   Aberdeen Proving Ground, Maryland 21005
   Attn: Dr. D. Eccleshall (DRXBR-BM)

5. Ballistic Missle Defense Advanced Technology Center
   P. O. Box 1500
   Huntsville, Alabama 35807
   Attn: Dr. L. Harvard (BMDSATC-1)

6. B-K Dynamics, Inc.
   15825 Shady Grove Road
   Rockville, Maryland 20850
   Attn: Mr. I . Kuhn

7. Intelecom Rad Tech
   P. O. Box 81087
   San Diego, California 92138
   Attn: Mr. W. Selph

8. Lawrence Livermore Laboratory
   University of California
   Livermore, California 94550
   Attn: Dr. R. J. Briggs
   Dr. Kelvin Neil
   Dr. T. Fessenden
   Dr. E. P. Lee

9. Mission Research Corporation
   735 State Street
   Santa Barbara, California 93102
   Attn: Dr. C. Longmire
   Dr. N. Carron

10. National Bureau of Standards
Gaithersburg, Maryland 20760
Attn: Dr. Mark Wilson
Dr. S. Penner

11. Science Applications, Inc.
1200 Prospect Street
LaJolla, California 92037
Attn: Dr. M. P. Fricke
Dr. W. A. Woolson

12. Science Applications, Inc.
Security Office
5 Palo Alto Square - Suite 200
Palo Alto, California 94304
Attn: Dr. R. R. Johnston
Dr. Leon Feinstein

13. Science Applications, Inc.
1651 Old Meadow Road
McLean, Virginia 22101
Attn: Mr. W. Chadsey

14. Science Applications, Inc.
8201 Capwell Drive
Oakland, California 94621
Attn: Dr. J. E. Reaugh

15. Naval Surface Weapons Center
White Oak Laboratory
Silver Spring, Maryland 20910
Attn: Mr. R. J. Biegalski
Dr. R. Cawley
Dr. J. W. Forbes
Dr. D. L. Love
Dr. C. M. Huddleston
Dr. G. E. Hudson
Mr. W. M. Hinckley
Mr. G. J. Peters
Mr. N. E. Scofield
Dr. E. C. Whitman
Dr. M. H. Cha
Dr. H. S. Uhm
Dr. R. Fiorito

16. C. S. Draper Laboratories
Cambridge, Massachusetts 02139
Attn: Dr. E. Olsson
Dr. L. Matson

17. M.I.T. Laboratories
P. O. Box 73
Lexington, Massachusetts 02173
Attn: Dr. J. Salah

18. Physical Dynamics, Inc.
P. O. Box 1883
LaJolla, California 92038
Attn: Dr. K. Brueckner

19. Office of Naval Research
Department of the Navy
Arlington, Virginia 22217
Attn: Dr. W. J. Condell (Code 421)

20. Avco Everett Research Laboratory
2385 Revere Beach Pkwy.
Everett, Massachusetts 02149
Attn: Dr. R. Patrick

21. Defense Documentation Center (12 copies)
Cameron Station
5010 Duke Street
Alexandria, Va. 22314
Attn: TC

22. Naval Research Laboratory
Washington, D. C. 20375
P. Palmadesso - Code 4780 (50 copies)
M. Lampe - Code 4792
S. Ossakow - Code 4780
M. Friedman - Code 4700.1
J. R. Greig - Code 4763
I. M. Vitkovitsky - Code 4770
J. B. Aviles - Code 4665
M. Haftel - Code 4665
T. Coffey - Code 4000
Superintendent, Plasma Physics Division - Code 4700 (25 copies)
P. Sprangle - Code 4790
Library - Code 2628
J. Brown - Code 4701
A. Ali - Code 4700.1
D. Book - Code 4020
J. Boris - Code 4020
I. Haber - Code 4790
S. Kainer - Code 4790
A. Robson - Code 4760
D. Colombant - Code 4790

23. Defense Advanced Research Projects Agency
1400 Wilson Blvd.
Arlington, VA 22209
Attn: Dr. J. Mangano
Dr. J. Bayless

24. JAYCOR
205 S. Whiting St.
Alexandria, VA 22304
Attn: Drs. D. Tidman
R. Hubbard
J. Guillory

25. JAYCOR
Naval Research Laboratory
Washington, D. C., 20375
Attn: Dr. R. Fernsler - Code 4770

26. SAI
Naval Research Laboratory
Washington, D. C. 20375
Attn: A. Drobot - Code 4790
W. Sharp - Code 4790

27. Physics International, Inc.
2700 Merced Street
San Leandro, CA
Attn: Drs. S. Putnam
E. Goldman

28. Mission Research Corp.
1400 San Mateo, S. E.
Albuquerque, NM 87108
Attn: Dr. Brendan Godfrey

29. Princeton University
Plasma Physics Laboratory
Princeton, NJ 08540
Attn: Dr. Francis Perkins, Jr.

30. McDonnell Douglas Research Laboratories
Dept. 223, Bldg. 33, Level 45
Box 516
St. Louis, MO 63166
Attn: Dr. Michael Greenspan

31. Cornell University
Ithaca, NY 14853
Attn: Prof. David Hammer
Prof. Ravi Sudan

32. Sandia Laboratories
Albuquerque, NM 87185
Attn: Dr. Bruce Miller
Dr. Barbara Epstein

33. University of California
Physics Department
Irvine, CA 92717
Attn: Dr. Gregory Bendord
Dr. Norman Rostoker

34. Massachussets Institute of Technology
Cambridge, Mass. 02139
Attn: Prof. R. Davidson
Prof. G. Bekefi

35. Ian Smith, Inc.
3115 Gibbons Drive
Alameda, Calif. 94501
Attn: I. Smith

36. Lawrence Berkely Laboratory
Berkely, CA 94720
Attn: D. Keefe
A. Faltens